Supporting information of

Silver Nanoplate Aggregations based Multifunctional Black Metal Absorber for Localization, Photothermic Harnessing Enhancement and Omnidirectional Light Antireflection

Xiao-Yang Zhang,[a,b,c] *Feng Shan,*[a] *Huan-Li Zhou,*[a] *Dan Su,*[b] *Xiao-Mei Xue,*[b] *Jing-Yuan Wu,*[a] *Yu-Zhang Chen,*[a] *Ning Zhaoa,*[b] *and Tong Zhang**[a,b,c]

[a] *Joint International Research Laboratory of Information Display and Visualization, School of Electronic Science and Engineering, Southeast University, Nanjing, 210096, People's Republic of China.*

[b] *Key Laboratory of Micro-Inertial Instrument and Advanced Navigation Technology, Ministry of Education, and School of Instrument Science and Engineering, Southeast University, Nanjing, 210096, People's Republic of China.*

[c] *Suzhou Key Laboratory of Metal Nano-Optoelectronic Technology, Suzhou Research Institute of Southeast University, Suzhou, 215123, People's Republic of China.*

Corresponding Author
*Email: tzhang@seu.edu.cn

1. Morphology investigation of the SNPAs layer

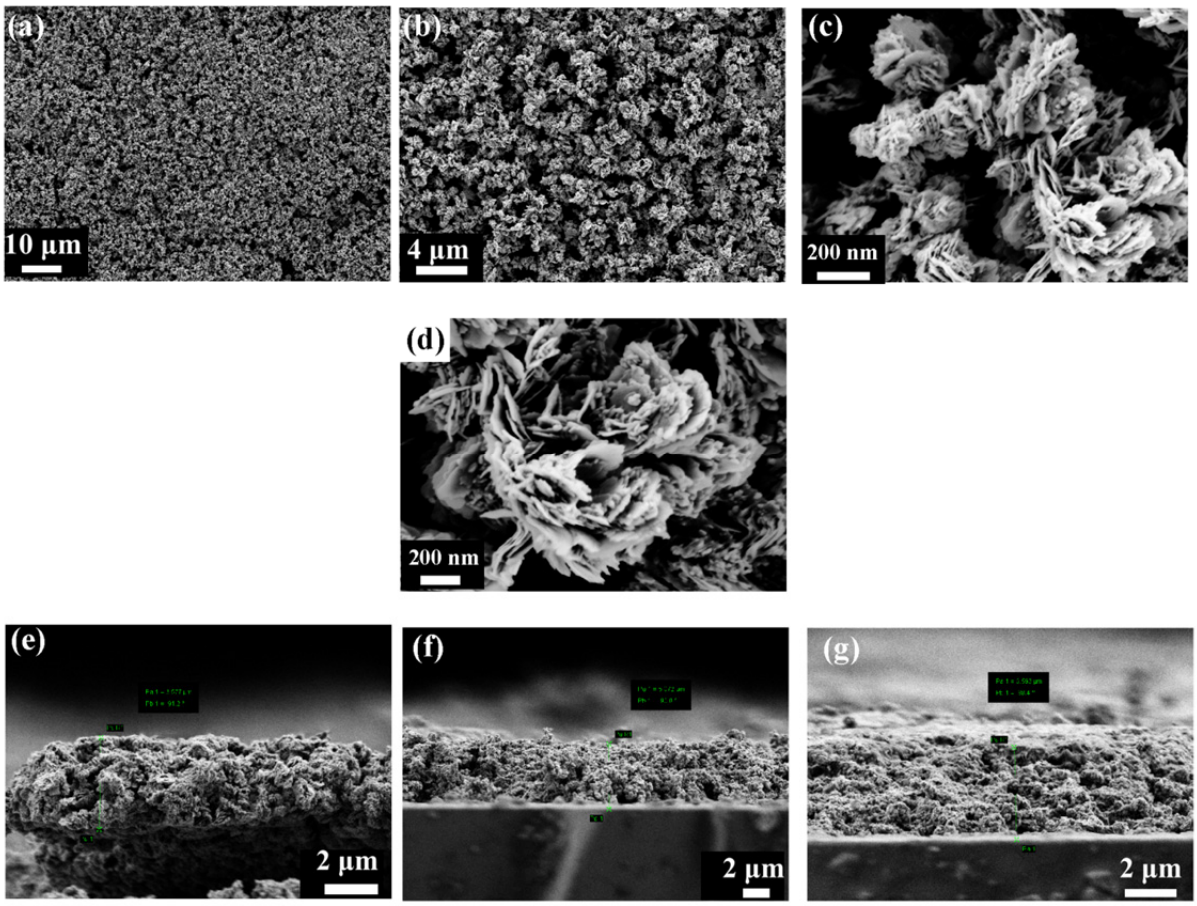

Figure S1. SEM images of the electrophoretic deposited SNPAs layer on ITO glass substrate. Images in (a)-(d) were taken from the top view. (e)-(g) were taken from the lateral view.

Images in Figure S1 show the detailed morphologic feature of the SNPAs layer. Figures S1a and b show that the SNPAs layer is uniform in large area. The layer was porous and constructed by randomly deposited SNPAs as shown in Figures S1c and d. The SNPAs were constructed by many silver nanoplates which were closely adjacent to each other. Figure S1d shows that many small spherical silver nanoparticles randomly embedded on the surfaces of nanoplates. Randomly

distributed cracks at the edges of silver nanoplates can be also easily observed. As the element constituting the observed nanostructures was silver as established by EDS analysis in Figure 2f, such silver nanostructures with various sub-wavelength morphologic features are unquestionable excellent plasmonic absorbers.

The thickness and surface roughness of the deposited SNPAs layer can be identified from Figures S1e-g. The thickness of the layer is between 3-5 µm.

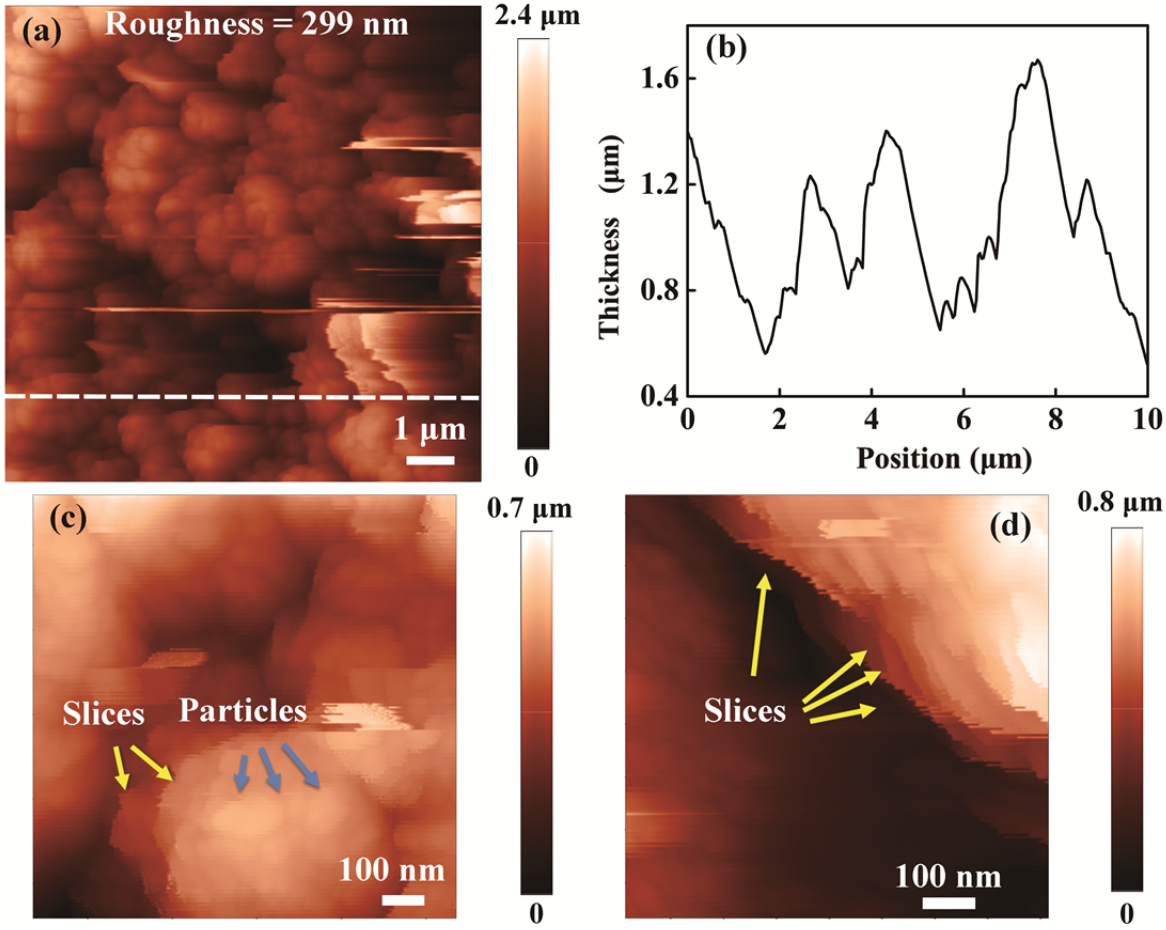

Figure S2. AFM images of the SNPAs layer. (a) shows morphology of the SNPAs layer in the large area. Lateral roughness shown in (b) was taken from the scanning line illustrated by white dash line in (a).

Atomic force microscope (AFM) (AFM module, NT-MDT NTEGRA Solaris) was used to

evaluate the surface roughness of SNPAs layer more accurately. A surface roughness of 299 nm was obtained from software statistics of large area AFM scanning result shown in Figure S2a. The lateral morphology of the layer taken from Figure S2a was shown in Figure S2b. The high surface roughness nature attributes to the porous structures constituted by the 3D structured SNPAs. This is also the reason why the SNPAs layer is super hydrophilic as demonstrated in Figure 7. Note that as the diameter of AFM prober is relatively large comparing with the morphologic features of SNPAs, the morphologic details of SNPAs can not be easily obtained from AMF images. However, the embedded spherical nanoparticles and the multilayer sheet structures can also be observed from the enlarged AFM images in Figures S2c and d, in accordance with SEM images shown above.

2. Comparison of optical imaging of SNPAs under microscopy

To show the difference between the optical images taken by different objective lenses, 4×objective lens (UPlanFL N, 4×／0.13, FN 26.5, OLYMPUS) and 100×objective lens (MPlanFL N, 100×／0.9, FN 26.5, OLYMPUS) were selected, respectively. White LED light[1] was used as illumination source passing through the same objective lens. Therefore, optical images taken by camera are primary back scattering light reflected from the surface of the samples. Both the electrophoretic deposited SNPAs layer on ITO glass and isolated SNPAs dropped on ITO glass after drying at room temperature were compared for imaging. For SNPAs layer shown in Figures S3a and b, the appeared different colors of SNPAs were clearly observed. Under the observation of 4×objective lens, SNPAs layer appeared much darker than that of the area of ITO glass. In contrast, SNPAs layer appeared much brighter compared with ITO glass under the observation of 100×objective lens. Similar phenomenon was observed when isolated SNPAs were used as shown in Figures S3c and d.

Under the observation of 4×objective lens, SNPAs appeared black. In contrast, they became multiple colors under the observation of 100×objective lens. Apparently, the multiple colors observed from optical image taken by 100×objective lens can be evidence that SNPAs are plasmonic structures with broadband scattering enhancement capacity. Similar plasmonic structures induced light scattering enhancement observed directly by optical imaging with high magnification lens has also been reported before.[2-5]

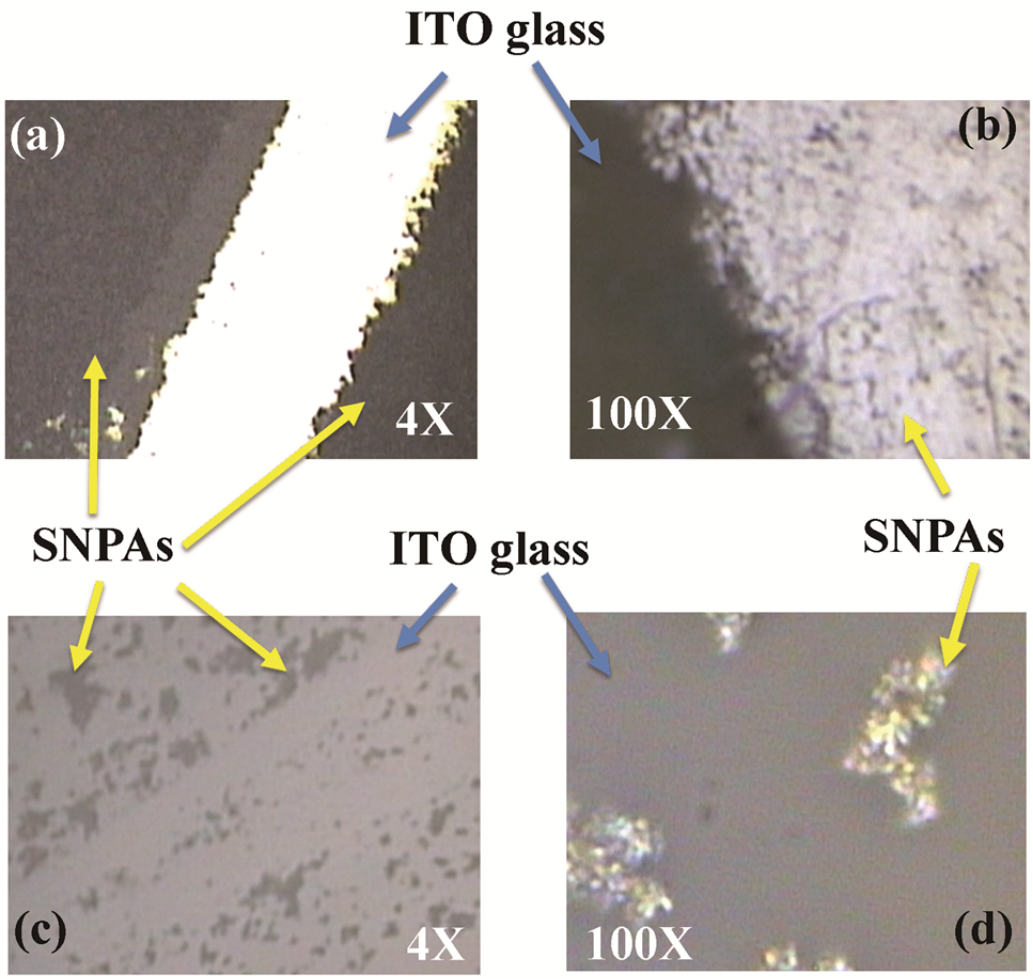

Figure S3. Comparison of optical images of SNPAs taken by 4×and 100×objective lenses, respectively. (a) and (b) show images of the electrophoretic deposited SNPAs layer using 4×and 100×objective lenses, respectively. (c) and (d) show images of isolated SNPAs dropped on ITO glass using 4×and 100×objective lenses,

respectively.

The reason why the color of SNPAs appeared different when 4× and 100×objective lens were used may attribute to their different light signal collection capacity. As the numerical aperture of 100×objective lens is 0.9 which is much larger than that of 4×objective lens used (0.13), more light signals scattered from plasmonic structures, i. e. SNPAs can be effectively collected by 100×objective lens. This optical imaging experiment can be an assisting method to understand the complicated interaction between SNPAs and light.

3. Distance dependent fluorescence excitation

To establish the existence of multiple LSPRs of SNPAs and show their near-field light localization and enhancement capacity, we performed a distance dependent fluorescence excitation experiment using quantum dots. The strategy of the experiment is illustrated in Figure S4. A layer of high transparent polymer isolator (NOA73, Norland Products) was spin coating on the surface of SNPAs layer. After ultraviolet curing of NOA73, quantum dots (commercial CdSe/ZnS quantum dots solution in toluene, 10 mg/mL, quantum yield of ~85% measured in solution, Suzhou Xingshuo Nanotech Co. Ltd.) were then spin coated (1000 rpm, 30 s) on the surface of NOA73. Photoluminescence of quantum dot–SNPAs layers samples were measured using confocal microscopic spectrometer, NT-MDT NTEGRA Solaris, as illustrated in Figure S4. 100× objective lens was used to focus light into small spot on the surface of SNPA layers. Then emission spectra of quantum dots samples were obtained as shown in Figure S5. The distance between quantum dots and SNPAs layer is dependent on the thickness of the NOA73 layer. By carefully controlling the spin coating processes (concentration of colloid and spin velocity), NOA73 layers with thickness of

30 nm and 170 nm were obtained. The thickness of NOA73 was measured using profilometer as shown in Figure S6. Two types of quantum dots with emission wavelength of 555 nm and 628 nm were used to test the wideband LSPR characteristic of SNPAs. For each samples, five positions were measured.

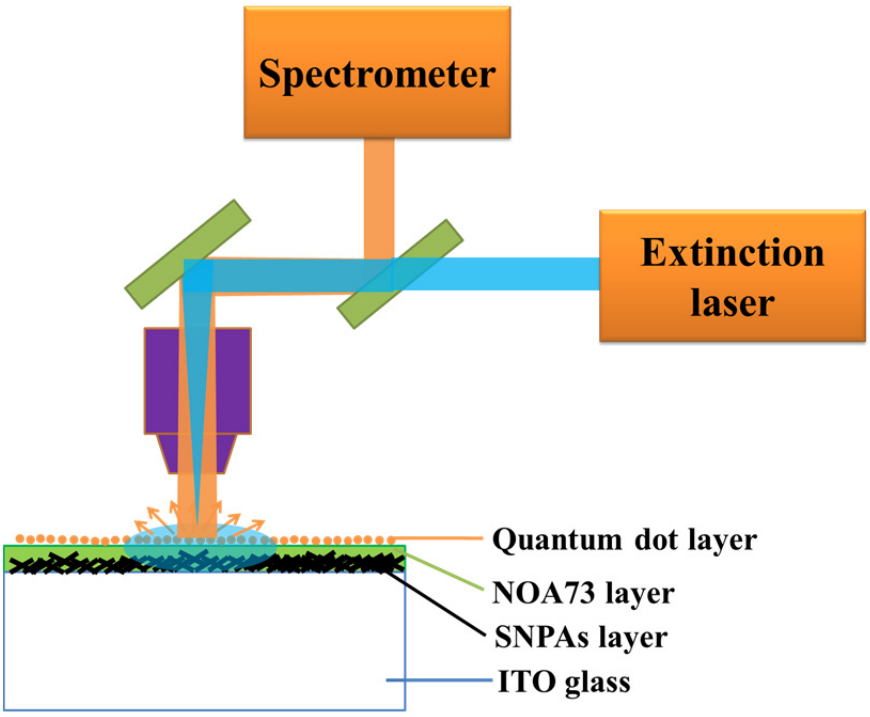

Figure S4. Schematic illustration of photoluminescence experiment

As shown in Figure S5a, when the distance between quantum dot layer and SNPAs layer is 30 nm, quantum dots can be efficiently excited by laser beam. However, emission of quantum dots layer became very weak when the distance between quantum dot layer and SNPAs layer slightly increased from 30 nm to 170 nm (which is still much shorter than the wavelength of excitation laser). The comparison results clearly confirmed that SNPAs can effectively localize light signals in near-field ranges owing to their LSPR property. Once the distance between quantum dots layer and SNPAs layer is increased to 170 nm, quantum dots can not be excited effectively either as

excitation light decayed rapidly away from the surface of plasmonic structures. We also observed emission intensity at different positions changed obviously for sample with thin layer of NOA73. This is reasonable because the surface of SNPAs layer is porous and locally inhomogeneous. However, as all the measured emission intensities (red curves) for sample with thin layer of NOA73 were much higher than that of sample with thicker layer of NOA73 (blue curves), the effectiveness of the photoluminescence experiment was confirmed.

When quantum dots samples with emission wavelength of 628 nm and excitation wavelength of 532 nm were used, similar result was obtained as shown in Figure S5b. It confirmed the broadband light localization property of SNPAs.

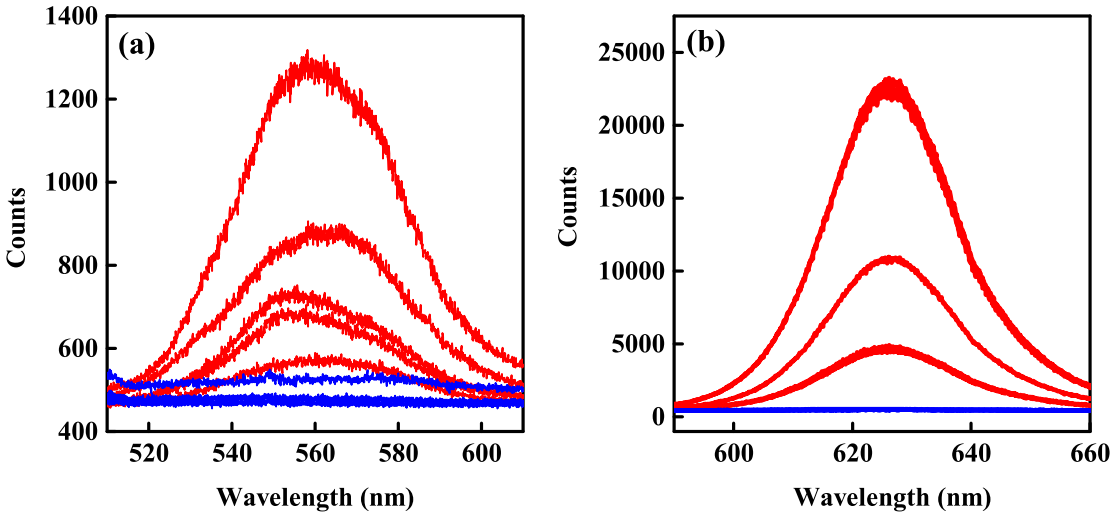

Figure S5. (a) Emission spectra of quantum dot layer excited by continuous laser with the wavelength of 473 nm and power of 41.5 μW. (b) Emission spectra of quantum dot layer excited by continuous laser with the wavelength of 532 nm and power of 2.6μW. Red curves and blue curves correspond to samples with an isolator layer of 30 nm and 170 nm, respectively.

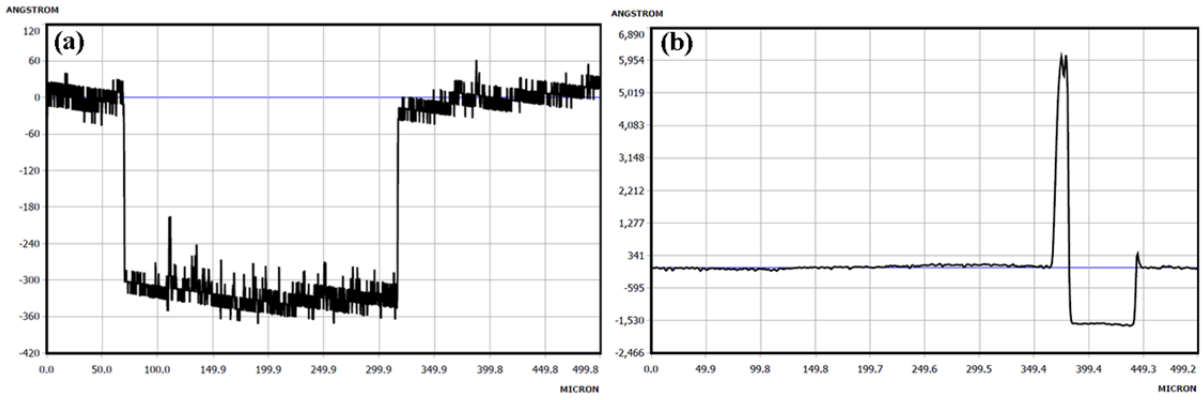

Figure S6. Thickness of NOA73 layers measured using profilometer. (a) and (b) show the thickness of two types of NOA73 layer used as isolator between SNPAs layer and quantum dots layer, respectively.

4. Numerical simulation of the SNPAs

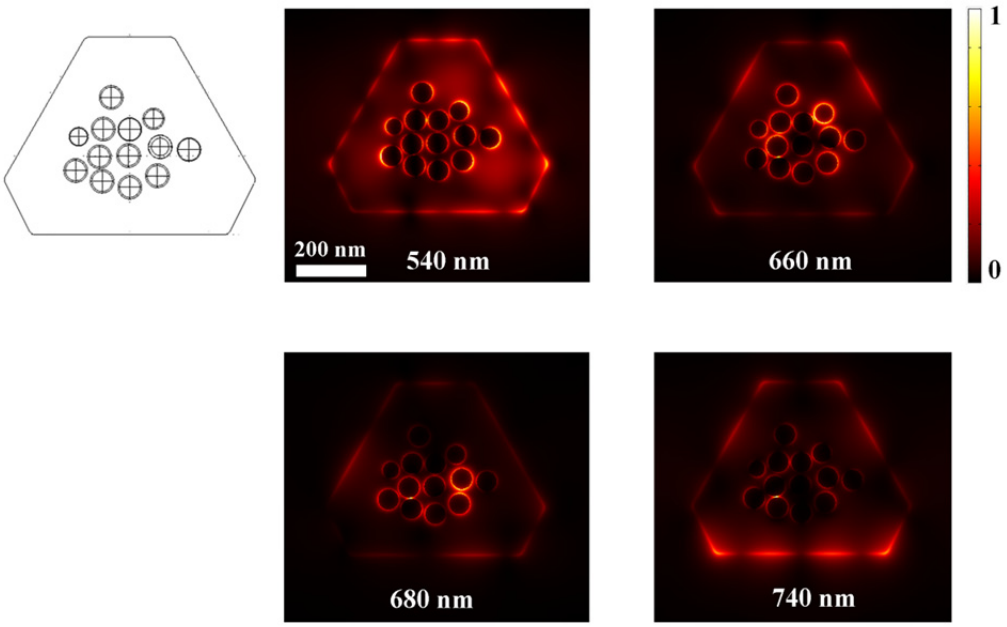

Figure S7. Normalized *E* field distribution of single silver nanoplate containing randomly embedded spherical nanoparticles. Excitation wavelength was labeled in the figures.

Figure S7 shows the 3D FEM simulation results of single silver nanoplate containing randomly embedded spherical nanoparticles on its surface. The diameter of these spherical nanoparticles

distributed in the range of 50 - 60 nm. The gap distance among these nanoparticles randomly distributed in the range of 5 nm - 10 nm. One can see clearly that hot spots randomly distributed in the gaps among these particles. When excitation wavelength changed, hot spots located at different areas can be observed easily. Apparently, the densely distributed spherical nanoparticles embedded on the surface of SNPAs attribute to the broadband light localization characteristic of SNPAs.

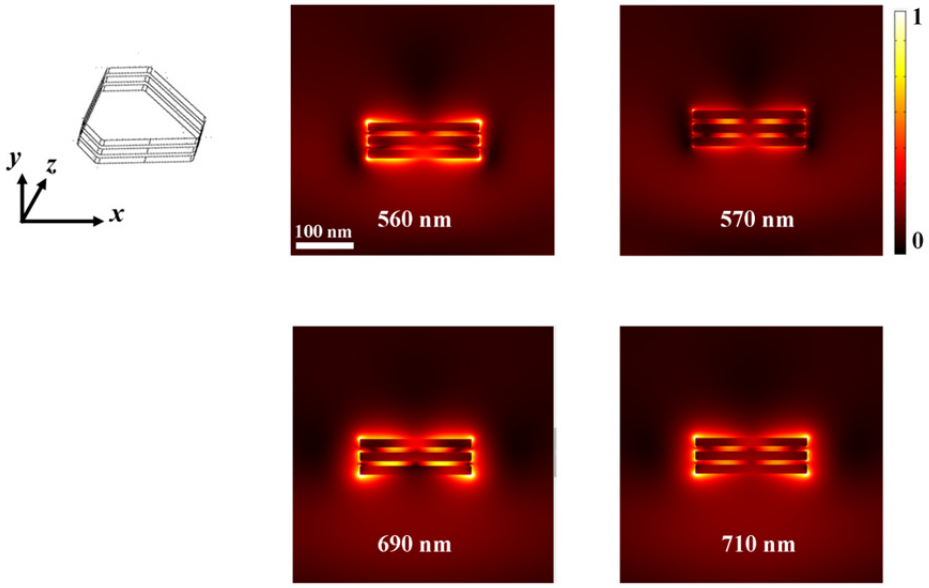

Figure S8. Normalized *E* field distribution (*x*-*z* plane view) of three closely adjacent silver nanoplates with a distance of 9 nm. The thickness of each nanoplate is 16 nm. The length of the size of the nanoplate is ~200 nm. Excitation wavelength was labeled in the figures.

Another morphologic feature of SNPAs is the nanoplates aggregations as illustrated in Figure S8. As shown from the 3D simulation results, light with different excitation wavelengths can be effectively trapped at the surface and gap areas when these nanoplates are closely adjacent. The *E*-field distribution became different when the excitation wavelength changed. These multiple light

trapping and coupling mechanism is the primary contribution to the broadband extinction of SNPAs.

5. Thermal stability test of SNPAs

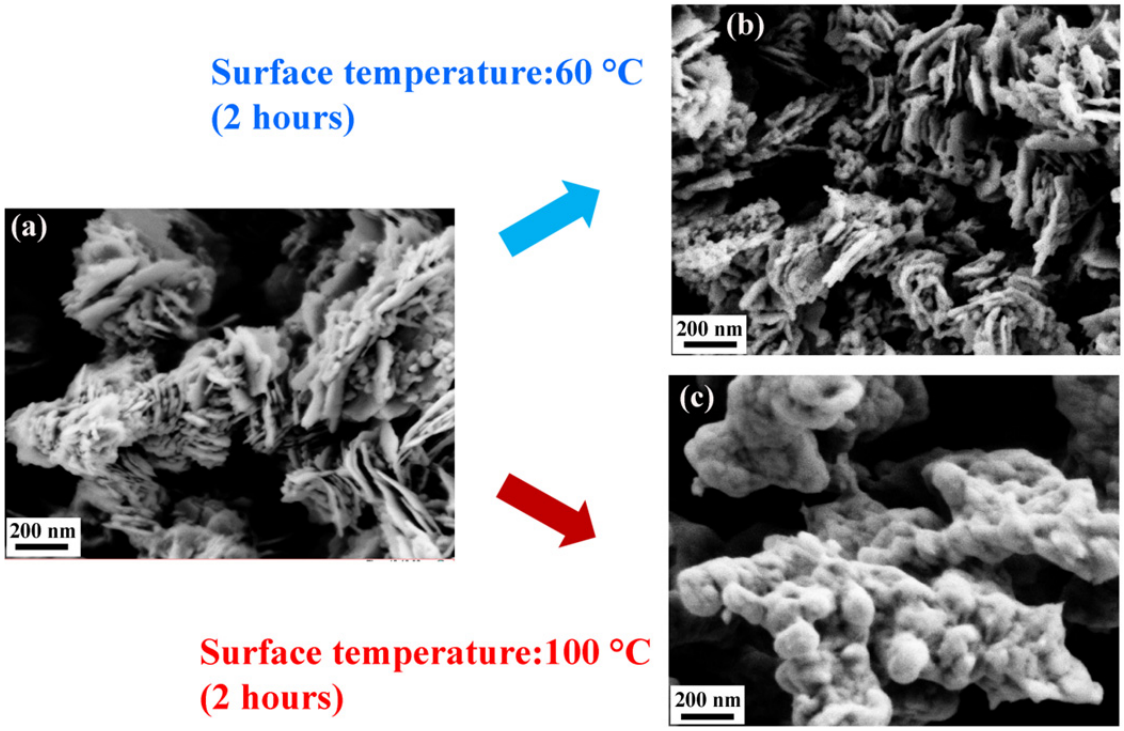

Figure S9. (a) SEM image of SNPAs layer without solar light illumination. (b) and (c) show the SEM images of SNPAs layer after 2 h illumination using solar light with different optical concentrations. The surface temperature was stabilized at 60 ℃ and 100 ℃ for (b) and (c), respectively.

References

[1] X. Y. Zhang, J. J. Xu, J. Y. Wu, et al. Seeds triggered massive synthesis and multi-step room temperature post-processing of silver nanoink—application for paper electronics, RSC Advances, 2017, 7(1): 8-19.

[2] X. Y. Zhang, A. Hu, T. Zhang, et al. Self-assembly of large-scale and ultrathin silver nanoplate films with tunable plasmon resonance properties. ACS Nano, 2011, 5(11): 9082-9092.

[3] E. Højlund‐Nielsen, J. Clausen, T. Mäkela, et al. Plasmonic colors: toward mass production of metasurfaces. Advanced Materials Technologies, 2016, 1(7).

[4] J. W. Stewart, G. M. Akselrod, D. R. Smith, et al. Toward Multispectral Imaging with Colloidal Metasurface Pixels. Advanced Materials, 2017, 29(6).

[5] J. M. Guay, A. C. Lesina, G. Côté, et al. Laser-induced plasmonic colours on metals[J]. Nature Communications, 2017, 8: ncomms16095.